Title:

Mechanisms of Airborne Infection via Evaporating and Sedimenting Droplets Produced by Speaking

Author(s):

Roland R. Netz

Citation:

"J. Phys. Chem. B 2020, 124, 33, 7093–7101 ; https://doi.org/10.1021/acs.jpcb.0c05229"

Mechanisms of Airborne Infection via Evaporating and Sedimenting Droplets Produced by Speaking

Roland R. Netz, Physics Department, Freie Universität Berlin, 14195 Berlin, Germany

Abstract*: For estimating the infection risk from virus-containing airborne droplets, it is crucial to consider the interplay of all relevant physical-chemical effects that affect droplet evaporation and sedimentation times. For droplet radii in the range 70 nm < R < 60 μm, evaporation can be described in the stagnant-flow approximation and is diffusion-limited. Analytical equations are presented for the droplet evaporation rate, the time-dependent droplet size and the sedimentation time, including evaporation cooling and solute osmotic-pressure effects. Evaporation makes the time for initially large droplets to sediment much longer and thus significantly increases the viral air load. Using recent estimates for SARS-CoV-2 concentrations in sputum and droplet production rates while speaking, a single infected person that constantly speaks without a mouth cover produces a total steady-state air load of more than 10^4 virions at a given time. In a mid-size closed room, this leads to a viral inhalation frequency of at least 2.5 per minute. Low relative humidity, as encountered in airliners and inside buildings in winter, accelerates evaporation and thus keeps initially larger droplets suspended in air. Typical air-exchange rates decrease the viral air load from droplets with an initial radius larger than 20 μm only moderately.*

1. Introduction

For understanding airborne viral infection pathways, the sedimentation properties of saliva droplets that contain non-volatile solutes and are subject to gravitational force, evaporation and evaporation cooling, are crucial. The typical considered droplet radii are less than 5 μm, because such droplets stay floating in air for many minutes even in the absence of evaporation. Aspects of this problem have been treated in previous experimental and theoretical works (1; 2; 3; 4; 5; 6; 7; 8; 9; 10) (11; 12; 13). Based on empirical expressions for the radius dependence of droplet evaporation and sedimentation times, Wells suggested that droplets with a radius smaller than 50 μm completely evaporate before falling to the ground and stay sedimenting as so-called droplet nuclei for a long time (2). In a seminal contribution, Duguid studied droplet sizes produced by humans sneezing, coughing and speaking from microscopic analysis of marks left on slides and found droplet radii between 1 and 500 μm (3). In fact, 95% of all particles had radii below 50 μm, and most final droplet radii were around 5 μm. Later studies basically confirmed these results and showed that in addition, many droplets are produced in the sub-micron radius range during coughing and speaking (14; 15; 16; 17; 18; 19). In a few studies multimodal droplet size distributions were found (20; 21), which has been rationalized in terms of distinct physiological droplet production mechanisms. In other studies it was shown that the number of droplets produced while speaking depends on the voice loudness (22) and that droplet production while exhaling is the product of complex fluid fragmentation processes (23). Recently, a much more sensitive method, time-resolved laser-light scattering, showed that far more droplets are produced than could be detected previously (24; 25), which demonstrates that the measured droplet radius distribution depends on the size sensitivity of the measurement technique used and also on the time droplets spend in air before measurement. The process of evaporation and sedimentation of saliva droplets involves diverse physical-chemical effects, such as high-Reynolds number effects for large droplets, finite evaporation-rate effects for small droplets, evaporation-

cooling effects and osmotic-pressure effects due to the presence of dissolved solutes. These effects are controlled by a large number of relevant parameters such as the initial droplet radius, the initial height at which droplets are produced, the ambient temperature, the relative humidity and the initial solute volume fraction, as schematically shown in Figure 1. The prevalent theoretical strategy in literature has been to deduce empirical relations or to numerically simulate evaporation and heat fluxes for selected parameter values. However, in order to estimate in the complete parameter space the number of virions that sediment in air given a certain droplet-production rate and a finite air-exchange rate in ventilated rooms, analytical formulas for the droplet evaporation and sedimentation times that explicitly depend on all relevant system parameters are crucial.

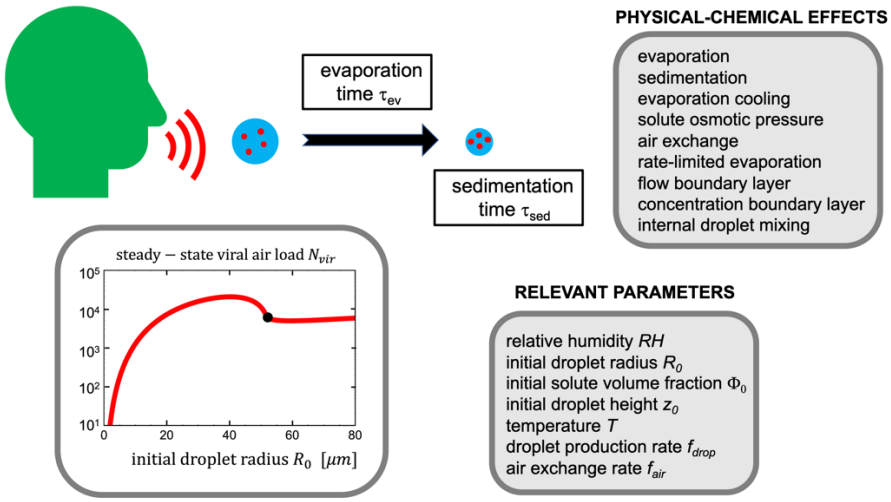

Figure 1: Overview over various physical-chemical effects and relevant parameters that control the evaporation and sedimentation times of saliva droplets and the viral air load due to speaking. The graph shows the steady-state number of virions sedimenting in air as a function of the initial radius of produced droplets due to a single infected person that constantly speaks and $RH = 0.5$, $\Phi_0 = 0.01$, $z_0 = 2$ m, T = 25°C, $f_{drop} = 1000\ s^{-1}$, $f_{air} = 10\ h^{-1}$.

In this paper, the physical-chemical mechanisms of evaporation and sedimentation of droplets with radii in the range from nm to a few hundred μm are considered, which is the range potentially relevant for airborne viral infection routes (26; 27; 28; 29). The analytical calculations include the interplay of all relevant physical effects: i) the finite evaporation reaction rate at the droplet surface, ii) the effects of relative humidity, iii) concentration-boundary as well as flow-boundary layers, iv) droplet cooling due to the large evaporation enthalpy of water, and v) the water vapor pressure reduction due to the presence of non-volatile solutes (including virions) in the droplet. Analytical expressions for the evaporation rate, the time-dependent droplet radius and the sedimentation time are derived in all relevant radius regimes as a function of all relevant parameters, from which estimates for the viral air load from speaking and the virion inhalation frequency in closed rooms including air exchange due to ventilation are derived.

Evaporation effects are typically treated on the level of the diffusion equation in the stagnant air approximation, i.e. neglecting the flow field around the droplet, and in the diffusion-limited evaporation regime. As shown here, this approximation is only accurate for droplet radii in the range 70 nm < R < 60 μm. Evaporation cooling is important and reduces the droplet surface temperature by about 10 Kelvin at a relative humidity (RH) of 0.5, which significantly slows

down evaporation. For radii larger than 60 μm, the air flow around the droplet speeds up the evaporation process and at the same time becomes non-Stokesian due to non-linear hydrodynamics effects, which is treated analytically by double-boundary-layer theory including concentration and flow boundary layers. For radii smaller than 70 nm, the evaporation at the droplet-air interface becomes reaction-rate limited. For these small droplets, the evaporation rate is not limited by the speed with which water molecules diffuse away from the droplet surface, but rather by the rate at which water evaporates from the liquid surface.

In the presence of evaporation, the sedimentation time is mainly determined by the final dried-out droplet radius, which depends on relative humidity and the initial solute concentration. Evaporation makes large droplets remain in air much longer and thus significantly increases the airborne viral load. Using recent estimates of the *SARS-CoV-2* concentration in sputum (30) and droplet production rates while speaking (24) (25), a single person that is infected and speaks constantly without a mouth cover is predicted to produce a steady-state airborne viral air load of more than 10^4 virions at a given time. In a mid-size closed room, this will result in a virion inhalation frequency by a passive bystander of at least 2.5 per minute, which is for initial droplet radii larger than 20 μm only moderately reduced by air-exchange rates in the typical range of up to about $20\,h^{-1}$. The quest for quantitative estimates of air-borne viral infection risks still faces many challenges but also provides highly relevant future research directions, as highlighted in this perspective.

2. Results

Droplet sedimentation and diffusion without evaporation. It is useful to first recapitulate a few well-known basic equations in the absence of droplet evaporation. By balancing the Stokes friction with the gravitational force, proportional to the acceleration g, that acts on a droplet with radius R and mass density ρ, the mean sedimentation time (see Supporting Information Section A) is

$$\tau_{sed} = \frac{k_B T z_0}{D_R m g} = \frac{9\eta z_0}{2\rho R^2 g} = \varphi \frac{z_0}{R^2} \qquad (1)$$

where the Stokes expression is used for the droplet diffusion constant $D_R = k_B T/(6\pi\eta R)$, the droplet mass is given by $m = 4\pi R^3\rho/3$, and values for the gravitational constant g, viscosity of air η, water density ρ, thermal energy $k_B T$ at 25°C are given in Table I. The numerical prefactor in eq 1 turns out to be ϕ = 0.85 x 10^{-8} m s. For a droplet with radius R = 5 μm placed initially at a height of z_0 = 2 m, the sedimentation time is τ_{sed} = 680 s = 11 minutes, other numbers are given in Table II. The droplet radius R = 5 μm is often defined as a threshold radius below which the sedimentation time is sufficiently long to be considered relevant for infections. An exact calculation of the sedimentation time distribution is given in Supporting Information Section A, which shows that the relative standard deviation of the mean sedimentation time is small for droplet radii larger than R = 10 nm. Thus, the mean sedimentation time, τ_{sed} in eq 1, is a good estimate of typical sedimentation times for all droplets with R > 10nm.

Inertial effects due to the acceleration of a droplet that is initially at rest occur over the acceleration time, which is

$$\tau_{acc} = \frac{mD_R}{k_B T} = \frac{2\rho R^2}{9\eta} = \xi R^2 \qquad (2)$$

where the numerical prefactor is given by ξ = 1.2 x 10^7 s m^{-2}. Even for large droplets with *R*=100 μm, the acceleration time is $\tau_{acc} = 0.12\ s$, showing that droplets rapidly reach their terminal velocity, so that acceleration effects can be safely neglected in the relevant radius regime.

The lateral diffusion length during the time a droplet is sedimenting in stagnant air is readily estimated. For this, the mean-squared diffusion length at the mean sedimentation time is calculated from $x_{diff}^2 = 2D_R\tau_{sed}$. Inserting the mean sedimentation time from eq 1 results in $x_{diff} = \sqrt{\frac{3k_B T z_0}{2\pi R^3 \rho g}}$, which for z_0 = 2 m yields x_{diff} = 0.63 mm for a droplet of radius *R* = 1 μm and x_{diff} = 2.0 cm for a droplet of radius *R* = 100 nm. The lateral diffusion of droplets with radii in the micrometer range during their sedimentation time is, therefore, very limited and will be dominated by the initial emission speed, air flow and convection effects.

Droplet evaporation without non-volatile solutes. The effect of evaporation decreases the droplet radius during its descent to the ground and therefore increases the sedimentation time. For evaporation of a droplet at rest, which defines the so-called stagnant-flow approximation, the time-dependent shrinking of the radius occurs in the diffusion-limited evaporation scenario, which is valid for radii larger than *R* = 70 nm, and is given by (see Supporting Information Sections B and C)

$$R(t) = R_0(1 - \theta\ t(1 - RH)/R_0^2)^{1/2} \qquad (3)$$

Here R_0 is the initial droplet radius and the numerical prefactor is given by

$$\theta = 2D_w c_g v_w \left(1 - \frac{\varepsilon_C \varepsilon_T}{1+\varepsilon_C \varepsilon_T}\right) = 4.2\ \times 10^{-10} m^2/s \qquad (4)$$

where θ has units of a diffusion constant. The values for the water diffusion constant in air D_w, the liquid water molecular volume v_w and the saturated water vapor concentration c_g at room temperature 25 °C are given in Table I. *RH* denotes the relative air humidity. The reduction of the water vapor concentration at the droplet surface due to evaporation cooling is described by the linear coefficient ε_C according to $c_g^{surf} \approx c_g(1 - \varepsilon_C \Delta T)$. Here c_g^{surf} denotes the water vapor concentration at the droplet surface, which has a temperature that is reduced compared to the ambient air (at a temperature 25 °C) by ΔT. The linear coefficient is given by $\varepsilon_C = 0.032$ (see Supporting Information Section C). The value of the temperature reduction at the droplet surface is obtained by solving the coupled heat-flux and water diffusion-flux equations in a self-consistent manner and turns out to be linearly related to the relative humidity as $\Delta T = \frac{\varepsilon_T(1-RH)}{1+\varepsilon_T \varepsilon_C} = 19.9(1 - RH)$, where the coefficient ε_T is given by $\varepsilon_T \equiv \frac{D_w c_g h_{ev}}{\lambda_{air}} = 55$ (see Supporting Information Section C). Interestingly, at zero relative humidity, *RH* = 0, the droplet surface is cooled by 20 K: While the cooling effect is quite significant, droplet freezing does not occur at room temperatures above 20°C (at lower temperatures evaporation-induced freezing can very well occur and slow down evaporation even more). The factor in eq 4 that accounts for the evaporation cooling effect is given by

$\left(1-\frac{\varepsilon_C\varepsilon_T}{1+\varepsilon_C\varepsilon_T}\right)=0.36$, so cooling considerably slows down the evaporation process and cannot be neglected (see Supporting Information Sections B and C for the derivation of eq 3). If the radius becomes smaller than 70 nm before the end of the drying process, a crossover to the reaction-rate limited evaporation regime takes place, as is discussed in Supporting Information Section D. For radii larger than 60 μm, the flow around the droplet speeds up the evaporation process and at the same time becomes non-Stokesian due to non-linear hydrodynamics effects, which can be treated analytically by double-boundary-layer theory including concentration and flow boundary layers (31), as discussed in Supporting Information Sections E, F, G, H, I. Internal mixing due to diffusion inside the droplet is sufficiently fast for droplet radii below roughly 100 μm and concentration inhomogeneities can be safely neglected (see Supporting Information Section J). It transpires that the stagnant flow approximation used to derive eq 3 is valid for the initial radius range between 70 nm and 60 μm, which includes the range that produces the largest viral air load, as will be shown below.

From eq 3 it is seen that the decrease in the radius starts slowly and accelerates with time, it is therefore dominated by the initial stage of evaporation. Because of this, the time for evaporation down to a radius at which osmotic effects due to dissolved solutes (including virions) within the droplet balance the water vapor chemical potential, can be approximated as the time needed to reduce the droplet radius to zero, from eq 3 given by

$$\tau_{ev}=\frac{R_0^2}{\theta(1-RH)} \qquad (5)$$

This relation has been used by Wells in his classical work (2), but the chosen prefactor was different due to the neglect of evaporation-cooling effects. Notably, the evaporation time in eq 5 increases quadratically with the initial droplet radius R_0, while the sedimentation time in eq 1 decreases inversely and quadratically with the radius. Thus, at a relative humidity of *RH* = 0.5, a common value for room air, a droplet with an initial radius of R_0 = 10 μm has an evaporation time of τ_{ev} = 0.48 s, but needs (neglecting the reduction of the radius) τ_a = 170 s to sediment to the ground. Consequently, it will dry out and stay floating for an even longer time, depending on its final dry radius. Other numerical examples for evaporation times are given in Table II.

To accurately calculate the critical initial radius below which a droplet completely dries out before falling to the ground, one needs to take into account that evaporation changes the diffusion constant and the gravitational force during sedimentation. As detailed in Supporting Information Section B, the sedimentation time in the presence of evaporation and a finite relative humidity *RH* < 1 is given by

$$\tau_{sed}^{RH}=\tau_{ev}\left[1-\left(1-\frac{2\varphi z_0}{\tau_{ev}R_0^2}\right)^{1/2}\right] \qquad (6)$$

By inserting eq 5 into eq 6 it is seen that in the limit *RH* = 1 the result of eq 1 is recovered. The critical radius is defined by the initial radius for which the droplet radius just vanishes as it hits the ground, it follows from equating eqs 5 and 6 as

$$R_0^{crit}=(2\varphi\theta z_0(1-RH))^{1/4} \qquad (7)$$

and is similar to the law established by Wells (2) by simply equating the sedimentation and evaporation times. For *RH* = 0.5 and z_0 = 2 m one obtains $R_0^{crit} = 52\ \mu m$: All droplets smaller than $R_0^{crit} = 52\ \mu m$ will dry out before they hit the ground. In the absence of non-volatile solutes, the droplets will thus disappear for radii smaller than R_0^{crit}. In airliners the relative humidity is substantially lower than 0.5; in fact, for completely dry air with *RH* = 0, the critical radius predicted by eq 7 increases to $R_0^{crit} = 61\ \mu m$. Note that the results presented here hold in still air; in ventilated rooms, convection due to air circulation will prevent some droplets from falling to the ground for a long time. Figure 2 shows droplet sedimentation times τ_{sed}^{RH} as a function of the initial radius R_0 according to eq 6 for an initial height of z_0 = 2 m for different relative humidities. In the limit *RH* = 1 no evaporation takes place and the result of eq 1 is recovered (thick black line). As the initial radius approaches the critical radius R_0^{crit}, given by eq 7 and indicated by a broken line, the droplet disappears. The thin solid colored lines denote the evaporation times according to eq 5, the crossing of the evaporation and sedimentation times happens at the critical radius. The qualitative shape of these curves has been empirically established by Wells (2).

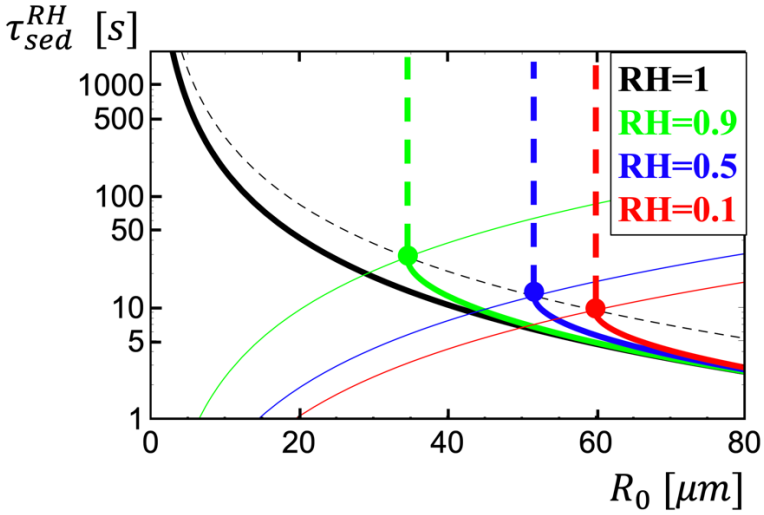

Figure 2: Sedimentation time of droplets τ_{sed}^{RH} in the presence of evaporation as a function of the initial radius R_0 in the absence of non-volatile solutes according to eq 6 for an initial height of z_0 = 2 m. Results are shown for different relative humidities, in the limit *RH* = 1 no evaporation takes place and the result in eq 1 is recovered (thick black line). As the initial radius approaches the critical radius R_0^{crit}, given by eq 7 and indicated by a black broken line, the droplets disappear (indicated by vertical broken lines). The thin solid colored lines denote the evaporation time eq 5.

Droplet evaporation in the presence of non-volatile solutes. The presence of non-volatile solutes in the initial droplet produces a lower limit for the droplet radius that can be reached by evaporation. Saliva contains a volume percentage of about 99.5 % water (32), the radius of a saliva droplet thus can maximally shrink by a factor $200^{1/3}$ = 5.8. Some of the water will stay inside the final droplet because of hydration effects. Assuming that the final state keeps 50% strongly bound hydration water, the droplet can thus maximally shrink by a factor of $100^{1/3}$ = 4.6 and the concentration of non-volatile solutes (including virions) increase by a factor of 100. Solutes in the droplet decrease the water vapor pressure, and therefore limit the droplet radius in evaporation equilibrium according to (see Supporting Information Section K)

$$R_{ev} = R_0 \left(\frac{\Phi_0}{1-RH}\right)^{1/3} \qquad (8)$$

Here, R_0 is the initial radius and Φ_0 is the initial volume fraction of solutes, including strongly bound hydration water. Only for *RH* = 0 does a droplet dry out to the minimal possible radius of $R_{ev} = R_0 {\Phi_0}^{1/3}$; for finite relative humidity the droplet in evaporation equilibrium is characterized by a solute volume fraction of $\Phi_{ev} = 1 - RH$. As an example, for *RH* = 0.5, the free water and solute (including hydration water) volume fractions in the equilibrium state equal each other. Equation 8 is modified for solutes that perturb the water activity, but for most solutes non-ideal water solution effects can be neglected.

Taking into account the water vapor-pressure reduction during the evaporation process, the radius-dependent evaporation time, which is the time it takes for the droplet radius to decrease from its initial value R_0 to R, is given by

$$t(R) = \frac{R_{ev}^2}{\theta(1-RH)}\left[\mathcal{L}\left(\frac{R_0}{R_{ev}}\right) - \mathcal{L}\left(\frac{R}{R_{ev}}\right)\right] \qquad (9)$$

as derived in Supporting Information Section K. Using a very accurate yet simple approximation for the scaling function $\mathcal{L}(x)$, eq 9 can be written as

$$t(R)/\tau_{ev} = 1 - \frac{R^2}{R_0^2} - \frac{2R_{ev}^2}{3R_0^2}\ln\left(\frac{R_0(R-R_{ev})}{R(R_0-R_{ev})}\right) \qquad (10)$$

where τ_{ev} denotes the evaporation time defined in eq 5. This expression demonstrates the logarithmic osmotic slowing down of the evaporation process due to the decreasing droplet water concentration as the droplet radius *R* approaches the equilibrium droplet radius R_{ev}. Neglecting this kinetic slowing down, which is represented by the last term in eq 10, one obtains the limiting result

$$t(R)/\tau_{ev} = 1 - \frac{R^2}{R_0^2} \qquad (11)$$

From this, an approximate expression for the evaporation time in the presence of solutes follows by setting $R = R_{ev}$ as

$$\tau_{ev}^{sol} = \tau_{ev}\left(1 - \frac{R_{ev}^2}{R_0^2}\right) \qquad (12)$$

which for small initial solute concentrations represents a minor correction to the evaporation time given by eq 5.

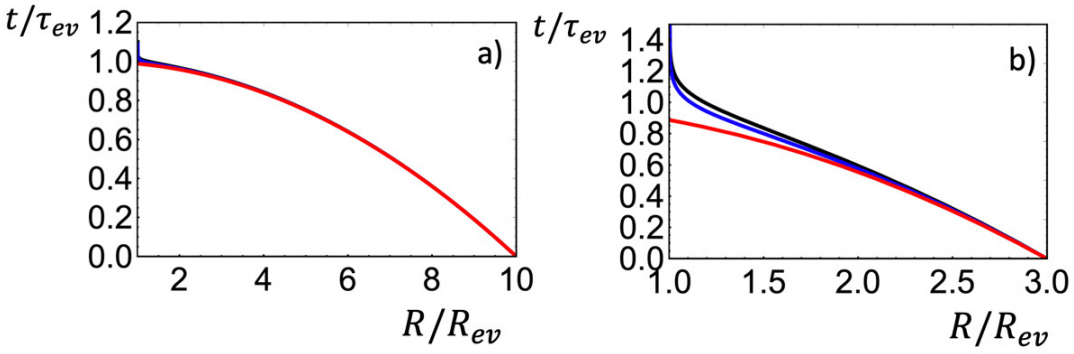

Figure 3: Scaling plot of the evaporation time *t(R)* as a function of the droplet radius *R* in the presence of solutes according to eq 9 (black lines). In a) the ratio of the initial droplet radius to the final equilibrium radius is $\frac{R_0}{R_{ev}} = 10$ and in b) this ratio is $\frac{R_0}{R_{ev}} = 3$. The red lines show the evaporation time when the water vapor-pressure reduction is neglected, eq 11; the blue lines show the approximation eq 10. The solute-induced water-vapor pressure reduction becomes significant only for radii close to the final equilibrium radius R_{ev} and leads to a diverging evaporation time.

Figure 3 shows the rescaled evaporation time as a function of the reduced droplet radius according to eq 9 as black lines. The presence of solutes only becomes relevant for droplet radii that are close to the final equilibrium radius R_{ev} and gives rise to a divergent evaporation time. Except for this final stage of evaporation, the formula eq 11 (red lines) describes the evaporation very accurately and will be used for all further calculations.

The sedimentation of not too large droplets thus can approximately be split into two stages: In the first stage, the droplets shrink down to a radius given by eq 8, and in a second stage the droplets sediment for an extended time with a fixed radius. The total sedimentation time follows as (see Supporting Information Section K)

$$\tau_{sed}^{sol} = \frac{\varphi z_0}{R_{ev}^2} - \frac{\tau_{ev}}{2}\left(\frac{R_0}{R_{ev}} - \frac{R_{ev}}{R_0}\right)^2 \qquad (13)$$

For droplets that are so large that they do not reach the radius R_{ev} before they hit the ground, eq 6 describes the sedimentation time very accurately.

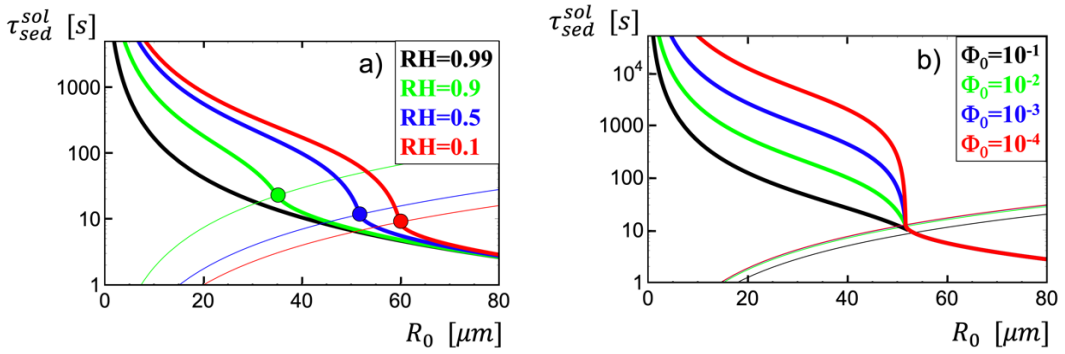

Figure 4: a) Sedimentation time of droplets τ_{sed}^{sol} as a function of the initial radius R_0 in the presence of non-volatile solutes with initial volume fraction $\Phi_0 = 0.01$ (which includes strongly bound hydration water) according to eq 13, for an initial height of z_0 = 2 m. Results are shown for different relative humidities, in the case *RH* = 0.99 no evaporation takes place and the result eq 1 is recovered (thick black line). The thin solid colored lines denote

the evaporation time eq 12. b) Sedimentation time of droplets τ_{sed}^{sol} as a function of the initial radius R_0 for fixed relative humidity *RH* = 0.5 and an initial height of z_0 = 2 m in the presence of non-volatile solutes with different initial volume fractions Φ_0 according to eq 13.

In Figure 4a the droplet sedimentation time τ_{sed}^{sol} is plotted as a function of the initial radius R_0 in the presence of non-volatile solutes with an initial solute volume fraction $\Phi_0 = 0.01$ and an initial height of z_0 = 2 m according to eq 13 for a few different relative humidities. For *RH* = 0.99 no evaporation takes place for $\Phi_0 = 0.01$, as follows from eq 8, and the result of eq 1 is recovered (thick black line). The thin solid colored lines denote the evaporation time eq 12. For small droplet radii, sedimentation is a two-stage process; droplets first evaporate down to the equilibrium radius R_{ev} and then stay floating in air for an extended time. Large droplets do not reach R_{ev} before they hit the ground, the transition between these two scenarios is illustrated by filled circles. In Figure 4b the droplet sedimentation time τ_{sed}^{sol} is plotted for fixed relative humidity *RH* = 0.5 and different initial solute volume fractions Φ_0. Figure 4 illustrates that the sedimentation times are significantly increased due to evaporation. In fact, as shown in Table II, for a relative humidity *RH* = 0.5 and $\Phi_0 = 0.01$, the sedimentation times of droplets increase for not too large radii by more than a factor of 10 due to evaporation.

Steady-state number of virions sedimenting in air. The virion content of a saliva droplet produced by an infected person is proportional to its initial volume. Denoting the droplet production rate of a single human who is speaking, which in principle depends on droplet radius, as f_{drop}, the number of humans that are simultaneously speaking as *m*, the virion number concentration in saliva as c_{vir}, the total number of virions sedimenting in air at a given time, denoted as N_{vir}, is in the steady state and in the absence of air exchange given by

$$N_{vir} = \frac{4\pi R_0^3}{3} \tau_{sed}^{sol}\, m\, f_{drop}\, c_{vir} \qquad (14)$$

and will be derived from the balance equation for the number of sedimenting droplets further below. In Figure 5a, the product of the initial droplet volume $\frac{4\pi R_0^3}{3}$ and the sedimentation time τ_{sed}^{sol} , which appears in eq 14 on the right side, is plotted as a function of the initial droplet radius for a few different relative humidities. This quantity shows for *RH* = 0.5 a broad maximum for initial droplet radii between roughly 5 μm and 50 μm. This interesting property is due to the fact that smaller droplets contain less volume but evaporate faster and thus have a longer sedimentation time. This means that the precise dependence of the droplet production rate f_{drop} on the initial droplet radius R_0 is not very important; the only important quantity is the total rate of droplets produced in the radius range between roughly 5 μm and 50 μm.

For the following estimate, the concentration of SARS-CoV-2 viruses in saliva will be assumed to be $c_{vir} = 10^6\ ml^{-1}$, which is a conservative estimate given the recent measurements of viral RNA concentration in human sputum, which yielded a mean value of $7 \times 10^6\ ml^{-1}$ (30). The droplet production rate from speaking was recently estimated in the droplet radius range between 12 μm and 21 μm as $2.6 \times 10^3\ s^{-1}$ (25) and in the radius range higher than about 20 μm as $\sim 10^3\ s^{-1}$ (24), from which the conservative estimate $f_{drop} \approx 10^3\ s^{-1}$ is constructed. Together this gives a factor $f_{drop} c_{vir} = 10^9\ s^{-1} ml^{-1} = 10^{-3}\ s^{-1} \mu m^{-3}$. For a single infected speaking human (*m=1*), this factor results in a steady-state number of virions floating in air between 10^4 and 10^5 for a humidity value around of *RH = 0.5* and for a radius

range between 5 µm and 50 µm, as follows from eq 14 and shown in Figure 5a on the right scale. This estimate does not depend on the room size (it also holds in open air) and assumes that the person does not wear a mask and is constantly speaking; obviously, it will be reduced if the person speaks only intermittently.

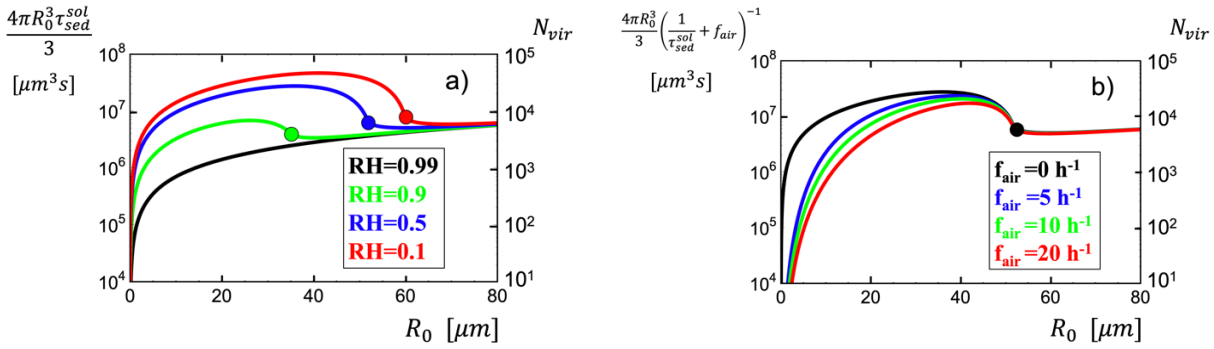

Figure 5: a) Product of the sedimentation time of droplets τ_{sed}^{sol} (given by eq 13) and the initial droplet volume $\frac{4\pi R_0^3}{3}$ as a function of the initial radius R_0 for an initial height of z_0 = 2 m and an initial solute volume fraction $\Phi_0 = 0.01$. Results are shown for different relative humidities, in the case *RH* = 0.99 no evaporation takes place and the result eq 1 is recovered (thick black line). The right scale shows the steady-state number of virions N_{vir} sedimenting in air assuming droplet production at a rate $f_{drop} = 10^3\ s^{-1}$ for a single droplet producer (*m* = 1) and for a saliva virion concentration $c_{vir} = 10^6\ ml^{-1}$ according to eq 14. b) Same as a) but including the effect of air exchange with a rate f_{air} according to eq 17. Results are shown for RH=0.5 and for four different air-exchange rates f_{air} in a closed room, assuming well-mixed air and a single droplet-producing speaking human, *m=1*.

In open air, the produced droplets will dilute due to the droplet-producing person moving around and due to wind and convection effects, here the droplet concentration is difficult to evaluate quantitatively. The situation in closed rooms can be analyzed in more detail. The balance equation that describes the time-dependent number of droplets sedimenting in a room is given by

$$\frac{dN_{drop}(t)}{dt} = mf_{drop} - \frac{N_{drop}(t)}{\tau_{sed}^{sol}} - N_{drop}(t)\, f_{air} \qquad (15)$$

The first term on the right side is the droplet production term, proportional to the droplet production rate f_{drop} and the number of droplet producers m. The second term is the droplet loss rate due to sedimentation to the ground, where it is assumed that air mixing does not modify the mean sedimentation time. The last term is the droplet loss rate due to air exchange that is proportional to the air-exchange rate f_{air}. In writing the last term, the assumption is made that the room air is well mixed, which should be a good approximation if the sedimentation time exceeds the time over which convection and ventilation effects mix the room air. Recommended air-exchange rates range from $f_{air} = 5/h$ in residential rooms up to $f_{air} = 20/h$ in multiply occupied offices and restaurants. In a steady state, the droplet number does not change with time and from eq 15 follows as

$$N_{drop} = mf_{drop}\left(\frac{1}{\tau_{sed}^{sol}} + f_{air}\right)^{-1} \qquad (16)$$

Thus, the steady-state total number of virions sedimenting in air follows as

$$N_{vir} = \frac{4\pi R_0^3}{3} c_{vir} N_{drop} = \frac{4\pi R_0^3}{3} c_{vir} m f_{drop} \left(\frac{1}{\tau_{sed}^{sol}} + f_{air} \right)^{-1} \qquad (17)$$

which is a generalization of eq 14 that includes air exchange. The steady state is reached after the relaxation time $\tau_{rel} = \left(\frac{1}{\tau_{sed}^{sol}} + f_{air} \right)^{-1}$, which is shorter than the sedimentation time τ_{sed}^{sol} and also shorter than the inverse air-exchange rate $1/f_{air}$. Thus, the steady-state number of sedimenting virions is reached rather quickly and is therefore of relevance. As is seen in Figure 5b, a finite air-exchange rate reduces the total number of virions floating in air significantly for small initial radii. However, the virion number from droplets with radii above $R_0 = 20\ \mu m$ is not affected much by a finite air-exchange rate, this is so because the sedimentation time in this range becomes shorter than the inverse air-exchange rate, which mitigates the air-exchange efficiency. Air recirculation between different rooms is a further risk, as it distributes the virion air load between all ventilated rooms.

An important question for infection-risk estimates is the number of virions that are inhaled by a person per minute. Denoting the tidal volume in normal breathing as V_{tidal}, the average respiratory frequency as f_{resp}, the room volume as V_{room}, the rate at which virions are inhaled by a person is given by

$$f_{inhale} = \frac{f_{resp} V_{tidal}}{V_{room}} N_{vir} = \frac{f_{resp} V_{tidal}}{V_{room}} \frac{4\pi R_0^3}{3} c_{vir}\ m\ f_{drop} \left(\frac{1}{\tau_{sed}^{sol}} + f_{air} \right)^{-1} \qquad (18)$$

where again the well-mixing assumption for air is used. The tidal breathing volume of adults is about $V_{tidal} = 0.5\ l$ and the average respiratory frequency is about $f_{resp} = 20/min$. Assuming a room volume corresponding to an area of 20 square meters and a height of 2 m, resulting in $V_{room} = 4 \times 10^4\ l$, the prefactor in eq 18 comes out as $\frac{f_{resp} V_{tidal}}{V_{room}} = 2.5 \times 10^{-4}\ min^{-1}$. As seen in Figure 5, the steady-state number of sedimenting virions is even for a single speaker (*m* = 1) larger than $N_{vir} \approx 10^4$ in the entire radius range between roughly $R_0 = 5\ \mu m$ and $R_0 = 50\ \mu m$ for a typical relative humidity *RH* = 0.5, corresponding to a virion concentration of $\frac{N_{vir}}{V_{room}} = 0.25\ l^{-1}$, and is only weakly reduced by increased air-exchange rates, as demonstrated in Figure 5b. The conclusion from eq 18 is that droplets produced by a constantly-speaking single infected person give rise to a virion inhalation rate of a passive bystander of at least $f_{inhale} = 2.5\ min^{-1}$ in a wide droplet radius range.

3. Discussion and Conclusion

It is gradually becoming acknowledged that airborne infection plays a crucial role in SARS-CoV-2 spreading (33; 34; 35) and that mouth covers could be instrumental (36; 37; 38), yet, it is not straightforward to derive the infection risk from the virion inhalation frequency given by eq 18. It is known that SARS-CoV-2 viruses remain viable in aerosols for at least 3 hours (26), which is longer than the sedimentation times in the relevant radius range, as seen in Figure 4. As a comparison, on inanimate surfaces these viruses stay infectious for days (26; 39). As a further complication, the relative humidity has a significant influence on virus stability, it was shown for bacteriophages and influenza viruses that stability is minimal at intermediate humidities around *RH* = 0.5 and is increased both for lower and larger humidities (40; 41).

Unfortunately, similar data is not yet available for SARS-CoV-2 viruses. Many factors determine the likelihood that a virus will spread from one person to another and that disease will result, but for other viruses it is known that inhaling as few as 5 virions can cause infection (42), so the above estimate of a virion inhalation rate of $f_{inhale} = 2.5\, min^{-1}$, which is a conservative estimate, should be relevant for the assessment of the viral airborne infection risk not only of SARS-CoV-2 but of other viruses as well.
From the analysis in this paper, it is clear that droplet sedimentation is a complex problem. In order to come up with analytical predictions, a number of simplifying assumptions had to be made. It has been assumed that diffusion within the droplet occurs quickly enough, so that the water concentration at the droplet surface does not differ significantly from the mean water concentration in the droplet. In Supporting Information Section J it is shown that this approximation should be valid for radii below R = 100 μm, which is larger than the relevant radius range for airborne infections. Surface tension effects, which increase the water vapor pressure, are negligible for droplets with radii larger than R = 1 nm, as explained in Supporting Information Section L. Likewise, the pressure increase due to evaporation and the change of droplet mass density with evaporation has been neglected.

Human sneeze was shown to produce a turbulent gas cloud of droplets mixed with hot and moist exhaled air, which can travel up to 8 m (43). It was demonstrated that the warm atmosphere in this cloud slows down evaporation for droplets that are small enough to reside inside the cloud for an extended time (44). The results presented here in principle hold also for droplets produced by sneezing once the droplets have left the sneeze cloud. Droplets larger than R = 100 μm quickly fall to the ground, but they can spread disease by ballistically landing on other people or on surfaces, which is a distinct infection mechanism and not considered here.

In summary, the evaporation of aqueous droplets with initial radii 70 nm < R_0 < 60 μm, can be described by the stagnant air approximation in the diffusion limit. These calculations demonstrate in terms of analytical formulas that droplets in the entire range of radii below $R_0^{crit} = 52\, \mu m$ for RH = 0.5, shrink significantly from evaporation before they fall to the ground and thus stay floating in air longer than their initial radius would suggest. This leads to a significant viral air load from droplets in the entire initial radius range 5 μm < R_0 < 50 μm, which includes the radius range of droplets produced by speaking (24) (25). A simple estimate of the viral inhalation frequency in a closed room suggests that 2.5 virions are inhaled per minute if one infected person is constantly speaking and not wearing a mask, typical air-exchange rates do not lower this number significantly. Thus speaking and presumably more so singing are shown to increase the risk of airborne viral infections substantially, which can be reduced efficiently by wearing a mouth cover (24) (25).
Future work along different lines is needed to address a number of important open questions: I) What is the precise size distribution of droplets produced by humans while speaking, while breathing and while physically exercising? What are the deviations among individuals, are there exceptional individuals that produce significantly more droplets than others? II) More statistics on the virus content of saliva as a function of the infection stage is direly needed, not only for SARS-CoV-2 but also for other viruses. III) Precise measurements of the times that viruses stay infectious in droplet nuclei for different temperatures and relative humidities. IV) How does the viscosity inside drying saliva droplets increase and how does that effect the evaporation kinetics? V) How effective are face masks of various fabrication specificities in filtering out droplets of different radii from speaking? VI) How is the sedimentation time

distribution calculated in Supplemental information Section A modified in the presence of convective and turbulent air-mixing effects? The analytical results presented in this work will hopefully stimulate and facilitate further research along these diverse directions.

Table I: List of numerical constants used (45).

k_BT	thermal energy	4.1 x 10^{-21} J at 25°C
η	viscosity of air	1.85 x 10^{-5} kg/ms at 25°C
η	viscosity of air	1.73 x 10^{-5} kg/ms at 0°C
ρ	liquid water density	997 kg/m^3 at 25°C
g	nominal gravitational constant	9.81 m/s^2
D_w	water diffusion constant in air	2.5 x 10^{-5} m^2/s at 25°C
D_w	water diffusion constant in air	2.2 x 10^{-5} m^2/s at 0°C
D_w^l	water diffusion constant in liquid water	$2.3 \times 10^{-9} m^2/s$ at 25°C
m_w	water molecular mass	2.99 x 10^{-26} kg
v_w	liquid water molecular volume	3.00 x 10^{-29} m^3 at 25°C
v_w	liquid water molecular volume	2.99 x 10^{-29} m^3 at 4°C
c_g	saturated vapor water concentration	7.69 x 10^{23} m^{-3} at 25°C
c_g	saturated vapor water concentration	1.62 x 10^{23} m^{-3} at 0°C
P_{vap}	water vapor pressure	3169 Pa at 25°C
P_{vap}	water vapor pressure	611 Pa at 0°C
ρ_{air}	density of air	1.18 x kg m^{-33} at 25°C
ν	kinematic air viscosity	1.6 x 10^{-5} m^2/s at 25°C
k_c	condensation reaction rate coefficient	370 m/s
a_{air}	air thermal diffusivity	2.1 x 10^{-5} m^2/s at 25°C
a_w	liquid water thermal diffusivity	1.4 x 10^{-7} m^2/s at 20°C
h_{ev}	molecular evaporation enthalpy of water	7.3×10^{-20} J at 25°C
h_{ev}	molecular evaporation enthalpy of water	7.5×10^{-20} J at 0°C
h_m	molecular melting enthalpy of water	1.0×10^{-20} J at 0°C
C_P^l	molecular heat capacity of liquid water	1.3×10^{-22} J at 20°C
λ_{air}	heat conductivity of air	0.026 W/mK at 25°C
λ_{air}	heat conductivity of air	0.024 W/mK at 0°C

Table II: List of representative sedimentation and evaporation times. R_0 denotes the initial droplet radius. τ_{sed} (*RH*=1) is the sedimentation time from a height of 2 meters without evaporation. τ_{ev} (*RH*=0.5) is the evaporation time at a relative humidity of *RH*=0.5 in the absence of non-volatile solutes in the droplet. τ_{sed}^{RH} (*RH*=0.5) is the sedimentation time in the absence of non-volatile solutes at a relative humidity of RH=0.5 from a height of 2 meters. τ_{sed}^{sol} (*RH*=0.5) is the sedimentation time from a height of 2 meters at a relative humidity of *RH*=0.5 in the presence of an initial volume fraction $\Phi_0 = 0.01$ of non-volatile solutes in the droplet.

R_0 $[\mu m]$	1	2.5	5	10	20	30	40	55
τ_{sed} $(RH = 1)$	5 h	45 min	11 min	170 s	43 s	19 s	11 s	5.6 s
τ_{ev} $(RH = 0.5)$	0.0048 s	0.030 s	0.12 s	0.48 s	1.9 s	4.3 s	7.7 s	14.5 s
τ_{sed}^{RH} $(RH = 0.5)$	∞	∞	∞	∞	∞	∞	∞	7.6 s
τ_{sed}^{sol} $(RH = 0.5)$	64 h	10 h	154 min	38 min	9 min	231 s	99.6 s	7.6 s

Acknowledgements: I thank William Eaton for helpful comments and for bringing this problem to my attention. Discussions with A. Bax, L. Bocquet, J.-F. Dufreche, I. Gersonde, P.

Loche, D. Lohse, T. Zemb are gratefully acknowledged. This research has been funded by the Max-Planck Water Initiative, by the Deutsche Forschungsgemeinschaft (DFG) through grant CRC 1114 "Scaling Cascades in Complex Systems", grant Number 235221301, Project C02 and by the ERC Advanced Grant No. 835117.

References

1. **Frössling, N.** Über die Verdunstung fallender Tropfen. *Gerlands Beitr. Geophysik.* 1938, Bd. 52, S. 170.
2. **Wells, W. F.** On Air-Borne Infection. Study II: Droplets and Droplet Nuclei. *Am. J. Hyg.* 1934, Bd. 20, S. 611.
3. **Duguid, J.P.** The size and the duration of air-carriage of respiratory droplets and droplet-nuclei. *J. Hyg.* 1946, Bd. 4, S. 471.
4. **Kinzer G. D. and Gunn, R.** The evaporation, temperature and thermal relaxation-time of freely falling waterdrops. *J. Meteorology.* 1951, Bd. 8, S. 71.
5. **Best, A. C.** The evaporation of raindrops. *Quart. J. Roy. Meteorol. Soc.* 1952, Bd. 78, S. 200.
6. **Ranz, W. E. and Marshall, W. R.** Evaporation from drops. *Chem. Eng. Progr.* 1952, Bd. 48, S. 141.
7. **Kukkonen, J., Vesala, T. and Kulmala, M.** The interdependence of evaporation and settling for airborne freely falling droplets. *J. Aerosol Sci.* 1989, Bd. 20, S. 749.
8. **Xie, X., Li, Y., Chwang, A. T. Y., Ho, P. ,L. and Seto, W. H.** How far droplets can move in indoor environments - revidsiting the Wells evaoporation-falling curve. *Indoor Air.* 2007, Bd. 17, S. 211.
9. **Liu, L., Wei, J., Li, Y. and Ooi, A.** Evaporation and dispersion of respiratory droplets from coughing. *Indoor Air.* 2017, Bd. 27, S. 179.
10. **Redrow, J., Shaolin Mao, S., Celik, I., Posada, J. A., Feng, Z.-G.** Modeling the evaporation and dispersion of airborne sputum droplets expelled from a human cough. *Building and Environment.* 2011, Bd. 46, S. 2042.
11. **Chong, K. L., Li, Y., Ng, C. S., Verzicco, R. and Lohse, D.** Convection-dominated dissolution for single and multiple immersed sessile droplets. *J. Fluid Mech.* 2020, Bd. 892, S. A21.
12. **Fuchs, N. A.** Evaporation and droplet growth in gaseous media. *Pergamon Press, London.* 1959.
13. **Parienta, D. et al.** Theoretical analysis of the motion and evaporation of exhaled respiratory droplets of mixed composition. *Journal of Aerosol Science.* 2011, Bd. 42, S. 1.
14. **Papineni, R. S. and Rosenthal, F. S.** The size distribution of droplets in the exhaled breath of healthy human subjects. *J. Aerosol Med.* 1997, Bd. 10, S. 105.
15. **Yang, S., Lee, G. W. M., Chen, C.-M., Wu, C.-C. and Yu, K.-P.** The size and concentration of droplets generated by coughing in human subjects. *J. Aerosol Med.* 2007, Bd. 20, S. 484.
16. **Xie, X., Li, Y., Sun, H. and Liu, L.** Exhaled droplets due to talking and coughing. *J. R. Soc. Interface.* 2009, Bd. 6, S. S703.
17. **Zhang, H., Li, D., Xie, L. and Xiao, Y.** Documentary research of human resipiratory droplet characteristics. *Proc. Eng.* 2015, Bd. 121, S. 1365.
18. **Chao, C. Y. H., Wan, M. P., Morawska, L., Johnson, G. R., Ristovski, Z. D., Hargreaves, M., Mengersen, K., Corbett, S., Li, Y., Xie, X., Katoshevski, D.** Characterization of expiration

air jets and droplet size distributions immediately at the mouth opening. *Aerosol Science.* 2009, Bd. 40, S. 122.
19. **Gralton, J., Tovey, E., McLaws, M.-L., Rawlinson, W. D.** The role of particle size in aerosolised pathogen transmission: A review. *Journal of Infection.* 2011, Bd. 62, S. 1.
20. **Johnson, G.R., Morawska, L., Ristovskia, Z.D., Hargreavesa, M., Mengersen, K., Chao, C.Y. H., Wan, M. P, Li, Y., Xie, X., Katoshevski, D., Corbett, S.** Modality of human expired aerosol size distributions. *Journal of Aerosol Science.* 2011, Bd. 42, S. 839.
21. **Somsen, G. A., van Rijn, C., Kooij, S., Bem, R. A. and Bonn, D.** Small droplet aerosols in poorly ventilated spaces and SARS-CoV-2 transmission. *Lancet Respir Med .* 2020, Bde. https://doi.org/10.1016/S2213-2600(20)30245-9.
22. **Asadi, S., Wexler, A. S., Cappa, C. D., Barreda, N. M., Bouvier, N. M. and Ristenpart, W. D.** Aerosol emission and superemission during human speech increase with voice loudness. *Scientic Reports.* 2019, Bd. 9, S. 2348.
23. **Scharfman, B. E., Techet, A. H., Bush. J. W. M. and Bourouiba, L.** Visualization of sneeze ejactat: steps of fluid fragmentation leading to respiratory droplets. *Exp. Fluids.* 2016, Bd. 57, S. 24.
24. **Anfinrud, P. A., Stadnytskyi, V., Bax, C. E. and Bax, A.** Visualizing speech-generated oral fluid droplets with laser light scattering. *New Engl. J. Med.* 2020, p. DOI: 10.1056/NEJMc2007800.
25. **Stadnytskyi, V., Bax, C. E., Bax, A., Anfinrud, P.** The airborne lifetime of small speech droplets and their potential importance in SARS-CoV-2 transmission. *PNAS.* 2020, Bd. 117, S. 11875.
26. **van Doremalen, N., Bushmaker, T., Morris, D. H., Holbrook, M. G., Gamble, A., Williamson, B. N., Tamin, A., Harcourt, J. L., Thornburg, N. J., Gerber, S. I., Lloyd-Smith, J. O., de Wit, E. and Munster, V. J.** Aerosol and Surface Stability of SARS-CoV-2 as Compared with SARS-CoV-1. *The new england journal of medicine.* 2020, Bd. 382, S. 16.
27. **Shamana, J., and Kohn, M.** Absolute humidity modulates influenza survival, transmission, and seasonality. *PNAS.* 2009, Bd. 106, S. 3243.
28. **Tellier, R.** Aerosol transmission of influenza A virus: a review of new studies. *J. R. Soc. Interface.* 2009, Bd. 6, S. S783.
29. **Ai, Z. T. and Melikov, A. K.** Airborne spread of expiratory droplet nuclei between the occupants of indoor environments: A review. *Indoor Air.* 2018, Bd. 28, S. 500.
30. **Wölfel, R., Corman, V. M., Guggemos, W., Seilmaier, M., et al.** Virological assessment of hospitalized patients with COVID-2019. *Nature.* 2020, Bde. https://doi.org/10.1038/s41586-020-2196-x.
31. **Batchelor, G. K.** An Introduction to Fluid Dynamics. *Cambridge University Press, Cambridge.* 1967.
32. **Humphrey, S. P., and Williamson, R. T.** A review of saliva: Normal composition, flow, and function. *The Journal of Prostethic Dentistry.* 2001, Bd. 85, S. 162.
33. **Morawska, L., Cao, J.** Airborne transmission of SARS-CoV-2: The world should face the reality. *Environment International.* 2020, Bd. 139, S. 105730.
34. **Zhang, R., Li, Y., Zhang, A. L., Wang, Y., Molina, M.J.** Identifying airborne transmission as the dominant route for the spread of COVID-19. *PNAS.* 2020, Bd. www.pnas.org/cgi/doi/10.1073/pnas.2009637117.
35. **Liu, Y., Ning, Z., Chen, Y., Guo, M., Liu, Y., Gali, N. K., Sun, L., Duan, Y., Cai, J., Westerdahl, D., Liu, X., Xu, K., Ho, K.-F., Kan, H., Fu, Q., Lan, K.** Aerodynamic analysis of SARS-CoV-2 in two Wuhan hospitals. *Nature.* 2020, Bde. https://doi.org/10.1038/s41586-020-2271-3.

36. **Leung, N. H. L. et al.** Respiratory virus shedding in exhaled breath and efficacy of face masks. *Nature Medicin.* 2020, Bde. https://doi.org/10.1038/s41591-020-0843-2.
37. **Stutt, R. O. J. H., Retkute, R., Bradely, M., Gilligan, C. A., Colvin, J.** A modelling framework to assess the likely effectiveness of facemasks in combination with 'lock-down' in managing the COVID-19 pandemic. *Proc. R: Soc. A.* 2020, Bd. 476, S. 20200376.
38. **Neupane, B. B., Mainali, S., Sharma, A., Giri, B.** Optical microscopic study of surface morphology and filtering efficiency of face masks. *PeerJ.* 2019, Bd. 7, S. e7142.
39. **Kampf, G., Todt, D., Pfaender, S., Steinmann, E.** Persistence of coronaviruses on inanimate surfaces and their inactivation with biocidal agents. *Journal of Hospital Infection.* 2020, Bd. 104, S. 246.
40. **Schaffer, F. L., Soergel, M. E., Straube, D. C.** Survival of Airborne Influenza Virus: Effects of Propa!]ating Host, Relative Humidity, and Composition of Spray Fluids. *Archives of Virology.* 1976, Bd. 51, S. 263.
41. **Lin, K., Marr, L. C.** Humidity-Dependent Decay of Viruses, but Not Bacteria, in Aerosols and Droplets Follows Disinfection Kinetics. *Environ. Sci. Technol.* 2020, Bd. 54, S. 1024.
42. **Musher, D. M.** How Contagious Are Common Respiratory Tract Infections? *The New England Journal of Medicine.* 2003, Bd. 348, S. 1256.
43. **Bourouiba, L.** A Sneeze. *The New England Journal of Medicine.* 2016, Bd. 375, S. e15.
44. —. Turbulent Gas Clouds and Respiratory Pathogen Emissions: Potential Implications for Reducing Transmission of COVID-19. *J. Am. Med. Assoc. .* 2020, Bd. DOI: 10.1001/jama.2020.4756.
45. **Lide, D. R.** CRC Handbook of Chemistry and Physics. 89 th Edition 2008.

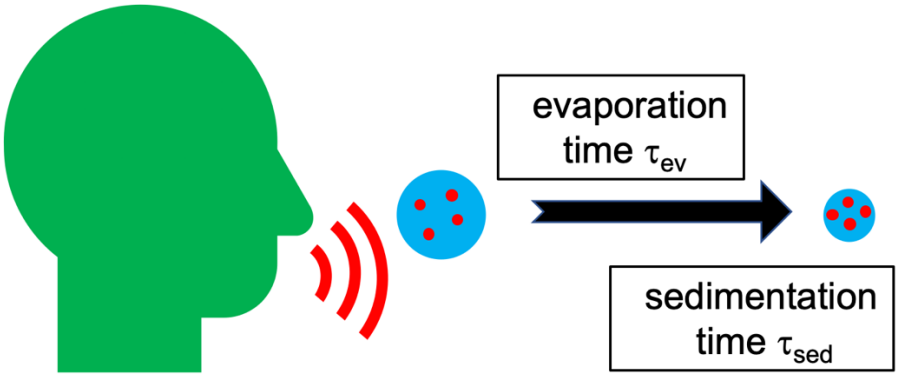

Table of content graphics